Imbibition or drying dynamics: Controlled by big and small capillaries interconnectivity

Rachid Bennacer, Xiaoyan Ma

Imbibition or Drying Dynamics: Controlled by Big and Small Capillaries Interconnectivity

Rachid Bennacer[1,2*], Xiaoyan Ma[2,3*]

[1]Tianjin Key Lab of Refrigeration Technology, Tianjin University of Commerce, P.R.C., 300134.
[2] Université Paris-Saclay, ENS Paris-Saclay, CNRS, LMT, Gif-sur-Yvette, France
[3] Beihang Hangzhou Innovation Institute, Yuhang, Hangzhou, China

*Corresponding author: rachid.bennacer@ens-paris-saclay.fr , ma.xiaoyan@ens-paris-saclay.fr

Abstract

In this work, we study the capillary rise mechanisms in heterogeneous porous material with different capillary sizes. Both theoretical and experimental work are performed to investigate the time evolution and the exchange at the interface of different porous media (different capillaries diameters). The first basic part contains the homogeneous capillary (without layer exchange), which is presented to distinguish the different characteristic times and the liquid capillary rise regimes. Considering gravity effect, shear stress and inertia, three regimes are distinguished theoretically and experimentally based on these two dimensionless parameters (**Bo** and **Ga**). Theoretical analysis and simulation results show the capillary rise in tendency and the appearance of oscillatory phenomenon. In the second part, the heterogeneous porous media are investigated. A multilayer domain is adopted to model the multiple distribution in capillary sizes. The interaction between these layers (different equivalent capillary sizes) demonstrate how the cooperation appears in nature so as to fit with the optimal situation of fast filling the porous media or the equivalent in drying. Experimental results on both homogeneous and heterogenous cases (corresponding to simple capillary rise and capillary rise with layer exchanges) have a favorable accordance with the theoretical analysis. The enhancement in imbibition has been demonstrated and explained as well.

Keywords: porous media; capillary rise; imbibition; interaction of multilayers; drying in porous material

1. Introduction

When a capillary or porous medium is brought into contact with a wetting fluid, the liquid spontaneously moistens the walls of the pores and invades the interior space. The capillary rise is one of the most common phenomena in nature and it provides information regarding the structuring of capillarity. This phenomenon is observed in many natural processes, physiological fields and human activities with plenty of technological applications. It is the capillarity that brings water to the upper layer of the soil, participates in the transport of the sap in the plants, and also ensures the functioning of the ball-point pens. Knowledge of the laws of capillarity is of vital importance in the recovery of petroleum, civil engineering, dyeing of fabrics, printing ink and various other applications.

This phenomenon is also widely encountered in nature (soil, building materials) and several applications, such as inkjet printing[1], [2], related thermal comfort as textiles [3], nature exploitation [4]–[6], cooling system heat

pipes [7], [8], energy production - fuel cell [9], [10] , and in recent hot topics of microfluidics [11]–[14], lab-on-chip devices [15]–[17]. Studies of capillary rise, whether slow or rapid, are important for the control and prediction of these phenomena. Historically the static mechanism of capillary rise has been widely studied, while the high dynamic part during the rise is a point of renewed interest recently. The early works of Lucas[18], Washburn [19], Bell and Cameron [20] have founded much of the theoretical framework of capillary dynamics.

The experimental work of Geovanni Borelli (1608-1675) established the relationship between the capillary diameter and the liquid height rise as $h \sim 1/r$. This has, for the first time, related the origin of the flow given by the forces of surface tension to the different phases presented in Laplace Law. The capillary phenomenon has been intensively studied and later completed with the transient aspect of the evolution towards the steady state, which is characterized by the maximum imbibition height expressed by Jurin law [21]. The transient rise of liquid in a cylindrical capillary involves several physical terms, and an increasing complexity has been involved in research works. The force balance model involves several forces: the surface tension, inertia, viscous and gravity. An extension exists to incorporate the reservoir feeding liquid into the capillary [22]. Under some conditions, the capillary driven by imbibition in a homogeneous porous medium follows diffusive dynamics, which is characterized by square root of time [23], [24]. This kind of diffusive dynamics for spontaneous imbibition fit with the Lucas [18] and Washburn [19]theory for a cylindrical capillary tube.

The height of liquid rise versus time can exhibit several time characteristics and when the viscous time scale is bigger than that of reaching the stationary level, some oscillatory behavior appears [24]. A dimensionless approach of the classical model was summarized in [25] and it showed how the problem can be generalized. The interaction with bulk inertia was also studied in [26], and on more local aspect, in the direct vicinity of the interface, numerical work using a volume of fluid (VOF) formulation was studied in [27]. Such dynamic rises based on average velocity could be affected by the flow irregularity, gas interaction or the slip conditions. This could modify the results quantitatively and qualitatively, such as the time evolution, the oscillatory solutions of the reference model and critical damping [28]. Contrary to the infinity liquid reservoir, or microgravity condition (drop tower), we studied also the effects of a limited reservoir extension interacting with the capillary and the free surface of such reservoir [23].

The imbibition is strongly dependent on the shape of the capillaries [27], [29]–[33], which makes the phenomena dependent on the considered porous media. In multi-dispersed granular porous media, both the transient flow and the reached level in steady state are modified. According to the morphology of homogeneous porous structure, the finer the gradation, the lower is the diameter, correspondingly the greater number of pores, and larger surface area. All these properties result in an enhanced surface tension effect, which will consequently induce the increase in capillary lift height [29]. The dynamic flow is directly related to the permeability, and also the function of porosity. For the same porosity, the dimensionless permeability of homogeneous particles and tubular geometries are very similar when the porosity is less than 20%. However, for higher porosity the specific surface and tortuosity become significant effecting factors. The dimensionless permeability of tubular geometry is approximately twice that of homogeneous particles [30], which is a consequence of less friction and less effect from tortuosity. The fracture porous media exhibits also some equivalence to the dispersed non-consolidated one [30], [31], [34].

The main remaining question in heterogeneous porous media is what will be the imbibition resulting dynamics, especially when the porous media is constituted by construction of subdomain of distinct porosity-permeability-tortuosity. The understanding of the involved physical phenomena can explain the special imbibition front evolution which is faster than the one obtained by the subdomains (homogeneous porosity-permeability) that are considered separately. This interaction between subdomain aims also to afford basis to explain the constant

drying behaviour observed in soils, in chemical process of dispersed media, in biomaterials, etc. These evaporation rates are directly controlled by the imbibition phenomena in predicting the necessary time allowing the liquid to reach the upper surface and induce the enhancement of the evaporation, and it controls also the mass flow rate of liquid rise feeding the upper surface. The evaporation rising liquid ceases to fit with the diffusion equivalent model due to spatial inhomogeneity and we will demonstrate that the porous media use the hierarchical structure (interconnection between the sub-domain of different porosity-permeability) for different goals in order to allow the optimal behaviour.

In this work, we discussed the flow and imbibition in heterogeneous porous media, as well as analytical and experimental imbibition over time in multilayer domain. Based on the observed and calculated results, we gave reasonable explanation of imbibition enhancement due to transversal flow from big to small pores. We have also explained predicted the faster imbibition phenomenon in heterogeneous domain.

Concerning the structure of this paper, followed by the first part devoting to the bibliographic analysis, a second part will be focused on the theoretical aspect in coupled porous media (idealised by two equivalent capillaries). After that, the experimental tests on both homogeneous and heterogeneous media will be carried out, analysed, and compared with the analytical theory. In order to have a better understanding of this phenomenon, one must understand and predict the competition of capillary rise in heterogeneous media. In this work, the capillary rise will be studied for various media with different particle sizes. The captured knowledge enable us to quantify the equivalent phenomena that occur in building materials. An experimental method is used to study the effect of different capillary dimensions as well as different liquid-gas (water-air) surface tensions on the rising dynamics and equilibrium height of the capillary rise.

2. Theory and modelling

We will recall firstly the theoretical model for a single capillary and discuss the dimensionless controlling parameters. Such equivalent capillary diameter will be defined as homogeneous domain. In the second part we will consider two domains of different equivalent diameters (heterogeneous domain). The model will be adapted to such situation where the two different domains exhibit different liquid rise versus time with possible liquid passing from one domain to the other.

Homogeneous domain

The imbibition of the wetting fluid in the porous media is based on the liquid rise in a single capillary tube. As previously mentioned, it has been intensively studied and completed the transient aspect of the evolution towards the steady state (final state, noted as steady state or "∞"). The origin of the flow can be easily determined by the forces of surface tension between different phases given in Laplace law, Eq.(1), and by maximum capillary height (z_{max} or z_{mx}), as expressed in Eq. (2).

$$\Delta P = \sigma\, cos(\theta)\left(\frac{1}{R_1} + \frac{1}{R_2}\right) \tag{1}$$

$$z_{mx}(\infty) = \frac{2\sigma \cos\theta}{\rho g R} \tag{2}$$

In which, R_1, R_2 are the two main radii of curvature of the surface at the considered point. σ is the surface tension of liquid water (N/m). θ denotes the contact angle. There are cases of extreme fluid-interface behavior: $\theta = 0°$ is the case of perfect wetting and by contrast, $\theta = 180°$ is the case of perfect non-wetting [32]. The transient rise of liquid in a cylindrical capillary involves several physical terms, including the surface tension, inertia, viscosity and gravity [18], [19], [33] and the inertia induced by the feeding liquid from reservoir

into the capillary [22]. A dimensionless approach of the classical model was summarized and it shows how the problem can be generalized [25]. Such dynamic rises based on average velocity could be affected by the flow irregularity, gas interaction or the slip. This could modify the results quantitatively and qualitatively, such as the time evolution.

The height of liquid rise over time is predicted by such dimensionless approach given in [25], [26], mentioning the different time characteristics, the possible oscillatory behavior [24], and the critical damping [28] when the viscous time scale is bigger than that of reaching the stationary level. The model and related variables are summarized below, and we will complete it with interacting different porous media.
The model can be used not only for the rise of liquid in a single capillary, but also for the imbibition of liquid into porous media with equivalent capillary radius. Fig. 1 shows the fundamental principle of the dynamics and the projection along the axis of ascent in the system. The z direction indicates the position of liquid rising interface, and it is involved in the system of the surface tension, viscosity, gravity, and inertia within the tube and the added mass induced by the reservoir feeding liquid (M_C, M_∞) into the capillary.

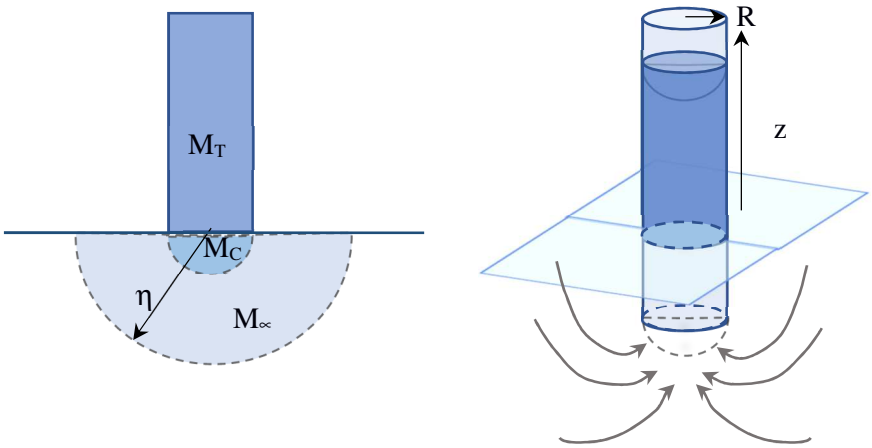

Figure 1. Illustration of the liquid rise and the different involved mass inertias

According to mass and momentum conservation law, the following equations can be deduced from the system:

$$(M_T + M_C + M_\infty)\frac{d^2z}{dt^2} = 2\pi R\sigma\cos\theta - M_T g - 2\pi R z\,\tau_{sh} - \pi R^2\frac{1}{2}\rho\left(\frac{dz}{dt}\right)^2 \quad (3)$$

In which,

$$(M_T + M_C + M_\infty) = \left(\rho\pi R^2 z + \frac{2}{3}\rho\pi R^3 + \frac{1}{2}\rho\pi R^3\right) \text{ and } \tau_{sh} = 4\mu\pi z\frac{dz}{dt}$$

M_T, M_C and M_∞ are the mass in the tube, the connecting spherical cap and the connecting domain to infinity, respectively (see Fig. 1). τ_{sh} represents the shear stress (friction), μ denotes the viscosity, R is the radius of the equivalent capillary tube, and z is the height in accordance to the capillary rise direction. Finally, we can obtain:

$$\frac{2\sigma\cos\theta}{\rho R} = gz + \frac{8\mu z}{\rho R^2}\frac{dz}{dt} + \frac{1}{2}\left(\frac{dz}{dt}\right)^2 + \left(z + \frac{7}{6}R\right)\frac{d^2z}{dt^2} \quad (4)$$

At the infinite time, $t = \infty$, the maximum height z_{mx} in steady state is given by Eq. (2). To generalize the problem, hereby we introduce dimensionless variables for time and space as $\tilde{z}$ and $\tilde{t}$, which are given by:

$$\tilde{z}(\tilde{t}) = z(t)/z_{mx} \text{ and } \tilde{t} = t/t_{r1}$$

Here we take t_{r1} as the reference time, which is based on inertial time, given by $t_{r1} = \sqrt{\frac{z_{mx}}{g}} = \sqrt{\frac{2\sigma\cos\theta}{\rho g^2 R}}$. The dimensionless transformation leads to the final general expression, as showed in Eq.(5). It is equivalent to the work in [22], and furthermore we integrate the contact angle in the dimensionless numbers.

$$1 = \left(\tilde{z} + \frac{7}{6}Bo\right)\ddot{\tilde{z}} + \frac{1}{2}\dot{\tilde{z}}^2 + \left(\frac{1}{8}\sqrt{Bo \cdot Ga}\right)^{-1}\tilde{z}\dot{\tilde{z}} + \tilde{z} \tag{5}$$

The two controlling parameters are distinguished in Eq. (5), which are the **Bond** number $\boldsymbol{Bo} = \frac{R}{z_{mx}} = \frac{\rho g R^2}{2\sigma\cos\theta}$, meaning the ratio between gravity and surface tension effect (contact angle is included within in the present number in our study) and the **Galileo** number $\boldsymbol{Ga} = \frac{gR^3}{\nu^2}$, representing the ratio of gravity to viscosity. Our ongoing study will concern mainly **Bo** <1, in order to get the significant vertical rise in comparison to the capillary radius and liquid used in our experiments.

To complete the previous chosen time scale reference, based on the dimensionless equation scale analysis $1 \sim \left\{ \underbrace{[z_{mx}/(g{t_r}^2)]}_{\substack{Inert.\ time \\ t_{r1}}} ;\ 8\underbrace{\left[\frac{z_{mx}}{g{t_r}^2}\right] t_r/(R^2/\nu)}_{\substack{Shear\ time \\ t_{r2}}} \right\}$, we have two other possible options for characteristic time, *i.e.* the diffusive reference time t_{dif} and the shear reference time t_{r2}. They are defined respectively by: $t_{dif} = R^2/\nu$; and $t_{r2} = \left[\frac{z_{mx}}{g}\right]\frac{8}{t_{dif}} = 8\frac{{t_{r1}}^2}{t_{dif}}$

Comparison of the three characteristic times (t_{dif}, t_{r1} and t_{r2}) as function of capillary radius is given in Fig. 2a. This figure illustrates the physical phenomena controlling the needed time for liquid rise regimes. For chosen liquid, the main controlling term (in Eq. 4 or 5) is dictated by the equivalent capillary radius. The calculation results (Fig. 2a) show that the chosen reference time t_{r1} is the least sensitive of the three to radius. The time to reach final asymptotic height is given for small radius by t_{r2} and by t_{r1} for the large radius. The corresponding Bo and Ga are plotted in Fig. 2b ($Ga^{\frac{1}{2}}$ as function of $Bo^{\frac{1}{2}}$ in logarithm axis). Our interested region, as previously mentioned, is where $Bo < 1$, as the dashed vertical line marked in Fig. 2b.

It's important to notice that the time ratio, corresponds to the identified characteristic number $\frac{t_{dif}}{t_{r2}} = \sqrt{Bo\ Ga} = \sqrt{\Omega}$, in the third term of right-hand side of Eq. (5). This Ω coefficient controls shear contribution in Eq. (5), so this term can be negligible for high values of $\sqrt{\Omega}$ and the oscillatory regime will appear (see[24]).

In order to make the $(Bo\ ;\ Ga)$ effect clearer, we plot in Fig. 2b, (mainly focus on region of $Bo < 1$, left region of the vertical dashed line), the three distinct domains based on the value of group $\sqrt{\Omega} = \sqrt{Bo \cdot Ga}$. We have a first domain (marked as purple area) with weak inertia ($Bo \cdot Ga \ll 1$), intermediate one ($Bo \cdot Ga \sim 1$) and the third with weak shear stress (the green region, $Bo \cdot Ga \gg 1$). In the same Figure (2b) we indicate also a set of square solid dots corresponding to the cases of water rise in capillary tube of different diameter from 0.02 to 4 mm (from left-down to right-up side).

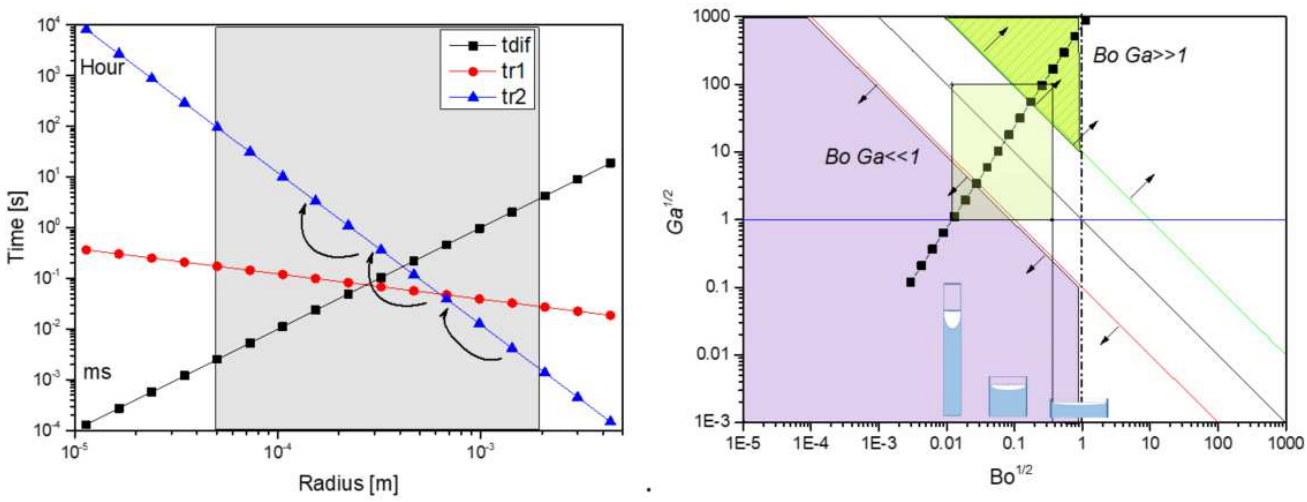

a) b)

Figure 2. The three involved characteristic times a), different regimes summarized by the two dimensionless numbers ($\boldsymbol{Bo}$; $\boldsymbol{Ga}$) b).

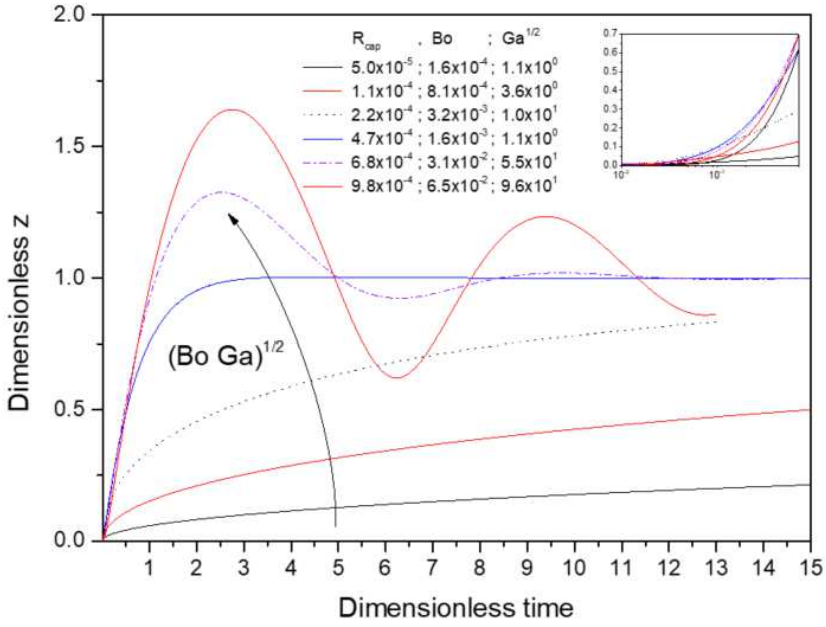

Figure 3. The capillary rise over time for different Ω

To illustrate more explicitly these three behaviors corresponding to the three regimes in Fig. 2b, we select cases from the solid dots plotted within the light green rectangle in Fig. 2b. The corresponding liquid rises over time in dimensionless scale are plotted in Fig. 3 for the chosen capillary diameters (corresponding to Bo and Ga *i.e.* Ω). These different curves are linked to increasing capillary radius (decreasing Ω) following the black curved arrow.

This figure summaries well the evolution tendency from the reduced dynamic rise profile (weak Ω) to the intermediate or moderate Ω (order of magnitude of one), where the three-time characteristics are comparable, and finally to the oscillatory regimes (high Ω). For moderate Ω, the time to reach the steady state is of order of magnitude of one (purple line), so we retrieve the time characteristic of 1 corresponding to the controlling phenomena (3 time characteristics of the same order - Fig. 2a, and center of the green square - Fig 2b, Ω ~1).

As t_{r1} decreases with the increase of radius (see Fig. 2a), we have faster tendency to reach the steady state with the increase of Ω until the oscillatory regime settles.

Heterogeneous domain

Consistently in the experimental work, we will study the liquid rise in porous media containing spherical particles (water in sand), which is corresponding to weak Ω. Experimental results of liquid rise in capillaries are numerous, with a large range of different situations including microgravity. A summary table can be found in [35]. As previously mentioned in our goals we will deal with heterogeneous sand layers as well. The sand will be considered firstly as equivalent homogeneous vertical capillary and the further objective focuses on the exchange between different layers (heterogeneous domain, multiple layers of different porous media).

As illustrated in Fig. 4a, the liquid rise in porous media is completely heterogeneous in a local point of view, as the capillary diameter is around an average equivalent radius but changing continuously in vertical direction. In addition, there exists also the interface interaction between the liquid and solid, which exhibits complex behaviour with locally concave ($R_i > 0$) and convex interfaces ($R_e < 0$), so that the related surface tension force strongly changes. The 3D complex interface in porous media can also exhibit a 2D interface shape within cracks, which is equivalent to infinity ($R_2 \to \infty$). We will consider only the equivalent capillary radius for a pile of sands to be comparable to a stack of perfect spheres in contact. By proceeding equivalence of surfaces, the radius of the equivalent capillary is based on adjusted geometrical aspect, as illustrated in the schematic diagram in Fig. 4b. The equivalent surface area ($S = \pi R_{cap}^2$) equals the equilateral triangle minus the 3 arcs of circles of diameter D and angle $\frac{\pi}{6}$. The equivalent capillary radius is given by Eq. (6).

$$R_{cap} = D\sqrt{\left(\frac{6\sqrt{3}}{\pi} - 3\right)/24} \tag{6}$$

In which, R_{cap} is the equivalent radius of the capillary and D is the diameter of the sand.

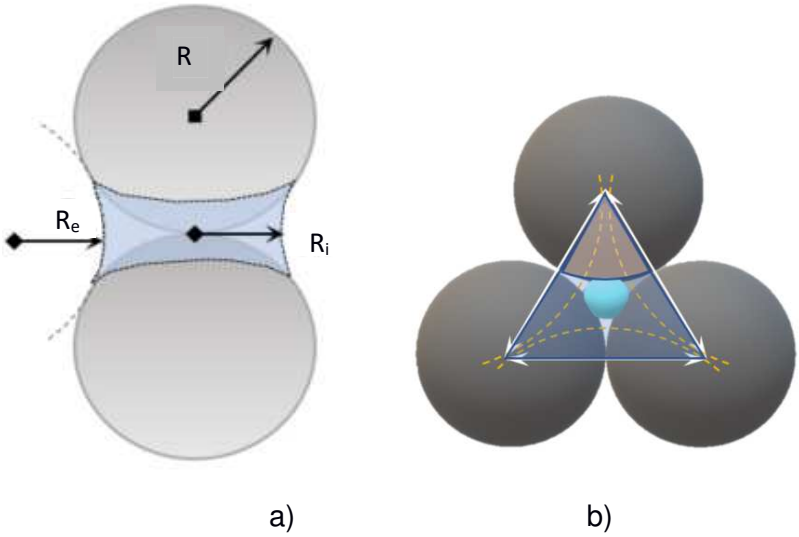

Figure 4. Liquid bridge and radii of curvature a) and the equivalent capillary radius [36]

In the present study, we aim to analyze the exchanges among the sub-structures of different capillary sizes (multilayer porous media). Therefore, we simplify the problem as multi-parallel layers of different diameter

sizes (Fig. 5a). Nevertheless, they are of the same porosity value because of the same type of spheres package. In each layer we have the liquid rise based on the layer equivalent radius and corresponding controlling parameter ($\Omega = Bo \cdot Ga$). Following the same model as previously described, we get equivalent system for the two layers (Fig. 5a) with equivalent radius denoted as R_1 and R_2 and corresponding liquid rise dimensionless heights noted as $\tilde{z}_1$ and $\tilde{z}_2$. Fig. 5b illustrates the connections between layers for horizontal liquid flow, and Fig. 5c shows the pressure profiles and induced difference at $\tilde{z}$ position along the capillaries before reaching the steady equilibrium height. This difference in pressure will induce liquid displacement in horizontal direction from one media (capillary) to the other. Such global exchange, or induced mass source, will modify the Eq. (6) and the evolution of the vertical position (capillary rise height) on both of the capillary layers. According to mass conservation law, the increase of mass in one capillary is equivalent to the decrease of mass in the other, *i.e.* positive and negative mass source for the corresponding capillaries.

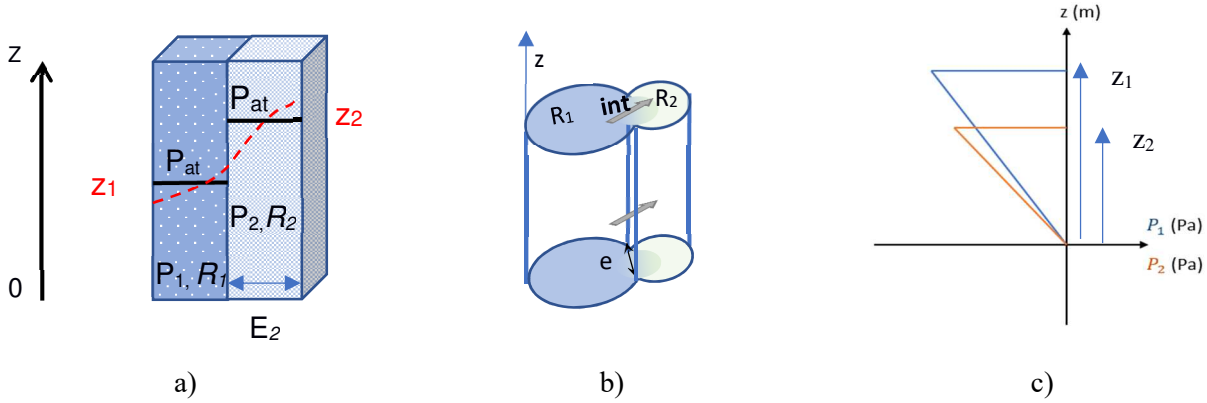

a) b) c)

Figure 5. Two layers of liquid exchange a), equivalent capillary case b), and the pressure on the two capillaries in vertical direction c)

We consider the pressure field as linear with the vertical position but it could be somehow different from the linear behavior at early time for important inertia term, *i.e.* small Ω case. The pressure difference between the two capillary centers versus the height can be estimated as:

$$\Delta P_{c1c2}(z) = \left(\frac{\Delta P_1^{\sigma}}{z_1} - \frac{\Delta P_2^{\sigma}}{z_2}\right) z = 2\sigma\left(\frac{\cos\theta_1}{R_1 z_1} - \frac{\cos\theta_2}{R_2 z_2}\right) z$$

In which, $z \in [0\,;\, z_{min}\,]$, and $z_{min} = \min(z_1, z_2)$, and it is the effective height below which the liquid exchange occurs between the two saturated adjacent layers. The induced horizontal flow is related to the pressure difference between interfaces, and related to the horizontal flow resistance (apparent permeability, K).

According to Darcy's law, the flow velocity $V_{int}(z)$ at the connecting interface can be expressed by:

$$V_{int}(z) = \frac{K_1}{\mu}\Delta P_{c1\_int}(z)/R_1 \;= \frac{K_2}{\mu}\Delta P_{c1\_int}(z)/R_2$$

therefore, the pressure between the center of the two layers is expressed using the interface position as:

$$\Delta P_{c1\_c2}(z) = \Delta P_{c1\_int} + \Delta P_{c2\_int} = \left(\frac{R_1}{K_1} + \frac{R_2}{K_2}\right)\mu\, V_{int}(z)$$

where ΔP_{c1_c2} is the pressure difference between the centers of two consecutive layers, so

$$V_{int}(z) = \frac{\Delta P_{c1\_c2}(z)}{\left(\frac{R_1}{K_1}+\frac{R_2}{K_2}\right)\mu} = \frac{\left(\frac{\Delta P_1^{\sigma}}{z_1} - \frac{\Delta P_2^{\sigma}}{z_2}\right)}{\mathcal{R}_{\text{eq}}} z \qquad (7)$$

where $\mathcal{R}_{\text{eq}}$ is the equivalent hydraulic resistance given by:

$$\mathcal{R}_{\text{eq}} = \left(\frac{R_1}{K_1} + \frac{R_2}{K_2}\right)\mu = \frac{R_1}{K_1}\left(1 + \frac{R_2 K_1}{R_1 K_2}\right)\mu$$

The volume flux transferred from layer (capillary) 1 to layer 2 through the connecting surface e, is given by:

$$\frac{dQv}{dt} = \int_0^{z_{min}} V_{int}(z) \cdot e \cdot dz = \frac{\left(\frac{\Delta P_1^\sigma}{z_1} - \frac{\Delta P_2^\sigma}{z_2}\right)}{\mathcal{R}_{\text{eq}}} e \cdot \int_0^{z_{min}} z.dz$$

Therefore, we deduce that:

$$\frac{dQv}{dt} = \frac{\left(\frac{\Delta P_1^\sigma}{z_1} - \frac{\Delta P_2^\sigma}{z_2}\right)}{\mathcal{R}_{\text{eq}}} \; e \cdot \frac{z_{min}^2}{2}$$

The extra mass balance on layer 1 will modify the liquid rise by a vertical velocity increase of:

$$\left(\frac{dz_1}{dt}\right)_+ \underbrace{\varepsilon * E_1}_{e} = -\frac{\sigma}{\mathcal{R}_{\text{eq}}}\left(\frac{\cos\theta_1}{R_1 z_1} - \frac{\cos\theta_2}{R_2 z_2}\right) e \cdot z_{min}^2$$

and the dimensionless form will be:

$$\left(\frac{d\tilde{z}_1}{d\tilde{t}}\right)_+ = -(Bo_1)^{-5/2}\sqrt{Ga_1}\; Bn_1.\left(\frac{1}{\tilde{z}_1} - \frac{R_{rel}}{cos\theta_{rel}}\frac{1}{\tilde{z}_2}\right)\tilde{z}_{min}^2 \tag{8}$$

Where $cos\theta_{rel}$ is the ratio of contact angle of two consecutive layers, *i.e.* we'll have the same contact angle and $cos\theta_{rel} = 1$ if same materials are used. Bn_1 denotes the horizontal flow coupling through the two-layer resistance (permeability) and the dimensionless surface connecting is represented by $\tilde{e}$.

$$Bn_1 = Da_{R1}\; \tilde{e} / \left(1 + \frac{K_{rel}}{R_{rel}}\right)$$

In which, we define: $R_{rel} = \frac{R_1}{R_2}$; $\cos\theta_{rel} = \frac{\cos\theta_1}{\cos\theta_2}$; $K_{rel} = \frac{K_1}{K_2}$; $Da_{R1} = \frac{K_1}{R_1^2}$; and $\tilde{z}_{min} = \min(\tilde{z}_0, \tilde{z}_1)$

The final system is the rewritten Eq (5) with the source term Eq.(8) for the two adjacent layers. The expressions are given below and could be solved by iteratively Euler explicit scheme.

$$\ddot{\tilde{z}}_1 = \left(1 - \frac{1}{2}\dot{\tilde{z}}_1^{\,2} - \left(\frac{1}{8}\sqrt{\Omega}\right)^{-1} \tilde{z}_1\, \dot{\tilde{z}}_1 - \tilde{z}_1\right) / \left(\tilde{z}_1 + \frac{7}{6}Bo\right)$$

$$\ddot{\tilde{z}}_2 = \left(\left(\frac{R\_rel}{\cos\theta_{rel}}\right) - \frac{1}{2}\dot{\tilde{z}}_2^{\,2} - \left(\frac{1}{8}\sqrt{\Omega}/R_{rel}^2\right)^{-1} \tilde{z}_2\, \dot{\tilde{z}}_2 - \tilde{z}_2\right) / \left(\tilde{z}_2 + \frac{7}{6}\left(\frac{Bo}{R_{rel}}\right)\right)$$

$$\dot{\tilde{z}}_1 = \int \ddot{\tilde{z}}_1 d\tilde{t} \quad \text{and} \quad \tilde{z}_1 = \int \left(\dot{\tilde{z}}_1 + \left(\frac{d\tilde{z}_1}{d\tilde{t}}\right)_+\right) d\tilde{t}$$

$$\dot{\tilde{z}}_2 = \int \ddot{\tilde{z}}_2 d\tilde{t} \quad \text{and} \quad \tilde{z}_2 = \int \left(\dot{\tilde{z}}_2 + \left(\frac{d\tilde{z}_2}{d\tilde{t}}\right)_+\right) d\tilde{t}$$

where $\frac{d\tilde{z}_2}{d\tilde{t}} = -\frac{d\tilde{z}_1}{d\tilde{t}} \cdot \tilde{e}_{rel}$

We present in Fig. 6 the evolution of liquid rise for two media (equivalent capillaries) named 1 and 2 for equivalent radius ratio of 1.1/4.7. Consequently, the maximum height of the considered reference $\tilde{z}_1$ will be 1 and the $\tilde{z}_2$ will be 0.23 (corresponding to 1.1/4.7). Fig. 6a is the dimensionless capillary rise height without exchange between the two layers. The important behavior is the fast filling of porous media 2 and reaching its maximum level ($\tilde{z}_2$ =0.23) with the order of magnitude 1 for the time scale. Meanwhile, porous media 1 reaches

higher $\tilde{z}_{mx}$ (~ 1), but in a longer time of more than one order of magnitude. We plot in the insert graphs of Fig. 6a, the corresponding pressure profile in both layers. The horizontal maximum change in each layer illustrates the pressure jump (Laplace law) and the increase with depth is the corresponding classical hydrostatic increases. It is apparent that the two layers exhibit two different pressure profiles. If the two adjacent consecutive porous media are not separated, a horizontal flow settle from one to the other in the direction of the pressure gradient.

Our main idea is to figure out the possible coupling between layers which allows to change the global dynamics of liquid rise in two adjacent layers. This behavior will explain the fast filling and high level of imbibition.
We will quantify and explain how the second layer (2), as fast filling layer, will feed the first layer (1) in order to evolve in the same time scale of order 1. Such coupling is a direct consequence of the vertical pressure profile plotted in the first insert graph at 'Early' time, as shown in Fig. 6a. We can see from the second insert graph 'Intermediate' time that the pressure profile remains favorable and is able to transfer liquid from layer 2 to layer 1. The two-layer liquid exchange will cease when the two layers reach the maximum height and consequently inducing no pressure difference on the vertical connecting surface (see the third insert graph in Fig. 6a).

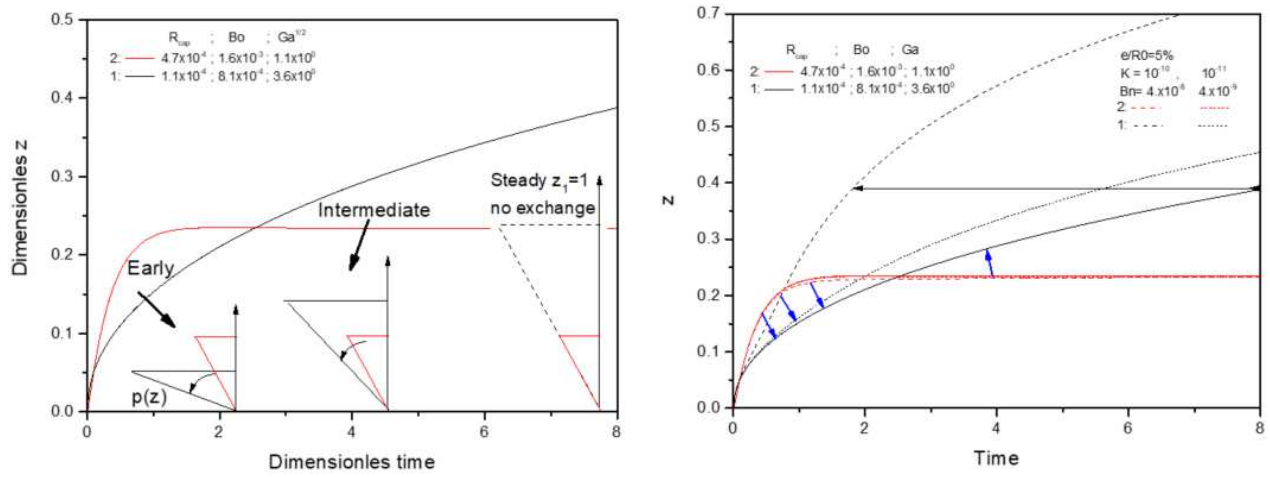

Figure 6. Liquid height versus time for two adjacent layers of different equivalent radius, without horizontal exchange (impermeable on the interface) a) and with exchange (permeable) b)

If we define the independent layers as impermeable, which means there is no horizontal exchange between layers (as illustrated in Fig. 6a), then Fig. 6b presents the evolution of liquid rise for the same two porous media but in case of permeable (exchange of liquid between the two layers, horizontal permeability).

The previous pressure coupling (plotted in Fig. 6a) in case of communicating layers is illustrated in Figure 6b. In this figure, we include the decoupled case (impermeable) represented by solid lines and we add the coupled ones with dashed lines. The layer 2 (red) is at higher z than layer 1(black) at the same time point in the beginning period, and this difference in pressure will induce liquid transfer from layer 2 towards layer 1. Such water feeding permits significant acceleration of liquid rise in layer 1 (black dashed line). As a result, layer 1 tends to catch up with the evolution in layer 2, while layer 2 filling up is not significantly modified due to inner vertical velocity. The layer 1 is filled up continuously from layer 2, due to the fact that in early age the pressure difference is significant (see first insert graph of Fig. 6a). The difference decreases over time but the vertical exchange interface increases ($\tilde{z}_{min}$) and this explains why the trend of speeding up is maintained over a longer time. We can see from comparison of the two figures that the layer 1 reaches the dimensionless height level of 0.4 in dimensionless time of 1.5 in the permeable case instead of 8 in the independent case (impermeable).

These results illustrate clearly the ability of cooperative structure in enhancing the imbibition and the liquid transfer from bottom to up. This coupling is enhanced by weak horizontal hydraulic resistance. For the case of lower permeability, thicker layers or relatively weaker connection between the layers, it is illustrated by short dot lines in Fig. 6b. The decrease of permeability and section communication reduced considerably the water transfer from layer 2 to layer 1 at the level that the new system is closer to the impermeable case.

3. Experiment protocol

In order to study the relationship between the capillary rise (imbibition) and the porous media permeability we used different sizes of spheres (such packed shapes exhibit constant porosity and different permeability). The different sphere diameters (sands) are supposed to be homogeneous media inside each group. The different groups are for diameter ranges: 0 - 0.2 mm, 0.2 mm- 0.4 mm, 0.4 mm- 0.8 mm, 0.8 mm- 1.6 mm, 1.6 mm- 3.15 mm and 3.15 mm - 6.3 mm, respectively (as given in Fig. 7a). The obtained average diameter $d_{Avg}(\pm 33\%)$ of the sand media for the six groups are 0.1 mm, 0.3 mm, 0.6 mm, 1.2 mm, 2.4 mm and 4.7 mm, respectively. The composition of the classical sand used in building versus the different used average diameter is plotted in cumulative percentage in Fig 7b (semi-logarithm coordinate).

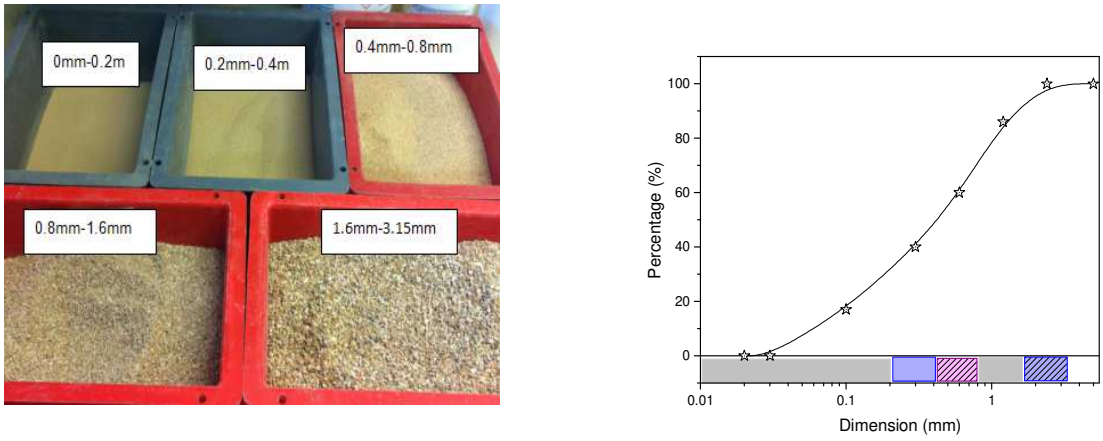

a) b)

Figure 7. Sands of different sizes after filtering a), Integral percentage of particle size curve b)

The imbibition (liquid rise) procedure consists of placing the sand layer in contact with the liquid and recording the induced capillary liquid rise. The setup is summarized in Fig. 8 where the two equivalent setups for homogeneous (Fig. 8a) and heterogeneous (Fig. 8b) domain are presented. The main difference between the homogeneous and heterogeneous experiments is the mass recording setup: a balance for the single homogeneous sands and a force sensor for the heterogeneous sands due to the heavier weight.

The experimental procedure of recording the imbibition (liquid rise) in the considered media combines two techniques:

- A force recording (balance or force sensor) relative to the suspended domain in which the liquid rise induces the mass evolution;
- An image processing of the movies which is visible for the wet sand in the transparent suspended domain.

The photo of the homogeneous case (Fig. 8a) shows the transparent suspended cylinder container with the testing sands inside. The cylinder is suspended and connected to the balance, which is recorded by computer

continuously. In addition, a digital camera is placed to record continuously the images as well. To keep the sands within the tube which is suspended by a wire to the balance (or the force sensor), a fine net filter has been designed and fixed on the underside of the setup (bottom of the tube or box that contains the sands).

For the heterogeneous case, the transparent box has a square section of 15 cm in width and a height of 60 cm. The box is filled with successive layers (each layer 2.5cm in width) of homogeneous sand and increasing average size of previously introduced 0.1 mm, 0.3 mm, 0.6 mm, 1.2 mm, 2.4 mm, and 4.75 mm. In view of the large mass of the device, it is impossible to use a balance and guarantee the precision, which leads us to build a frame equipped with a load sensor (500N), as presented in Fig. 8b.

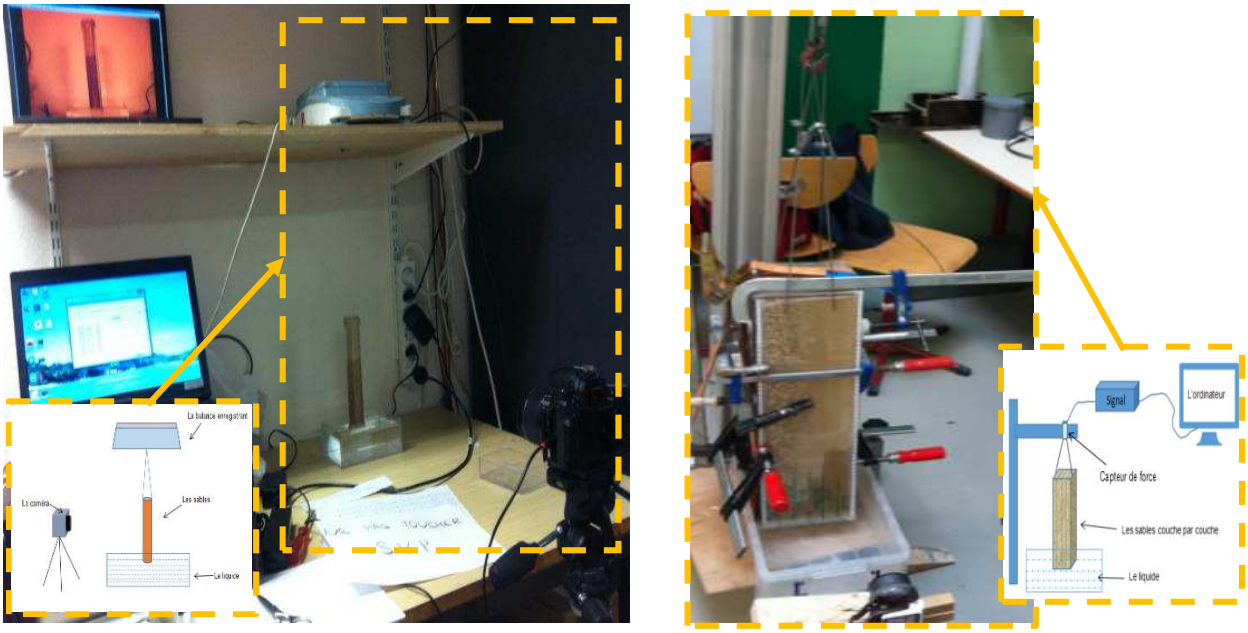

a) b)

Figure 8. Experimental devices for homogenous sands imbibition a) and heterogeneous with multi layers b), using balance or force sensor for mass recording and camera or capillary height monitoring

Results and discussion

At the considered initial time the liquid (water) is added to reach contact with lower part of the porous domain and the real-time mass is recorded by balance or force sensor. Meanwhile, a camera is used to record the liquid height inside the tube. We will present in this section the obtained results from the homogeneous and the heterogeneous domain (including 2 layers' interaction and 6 multilayers interactions). The evolutions of capillary rise are analysed and interactions between layers are discussed as well. For the homogeneous case, it is a validation procedure and we will confirm the accuracy of the used experimental technique, as well as the equivalent capillary diameter deduced from the sands.

Figure 9 represents the obtained results of maximum height for homogeneous domain. This figure represents both the visual capillary rise height recorded by the camera (represented by dots) and the height deduced from the obtained weight evolution of the absorbed liquid (represented by line). We include a few images at some time points to illustrate the obtained rise dynamics. Concerning the optical technique, it is explicit and therefore considered as a calibrating ruler. However, what we observe is the external surface, and we consider that the liquid level is the same on the horizontal plan. On the other hand, the weighting technique is able to provide the information of the liquid mass evolution. In order to convert the mass to height (proportional to volume and porosity), the section surface and the media porosity have been considered constant. For monodispersed spheres

the porosity does not depend on the sphere diameter but could depend on the type of arrangement. For arrangement styles of hexagonal compact, dense packaging, and hexagonal simple packing, the porosities are 26% 36% and 39%, respectively, and the porosity will decrease if it's not monodispersed spheres. For example, a bi-dispersed spheres of diameter ratio of 2 (the present used sand gap) will decrease the porosity by a factor of 0.9 [37]. We will consider in our case the porosity of order of 0.32. Some difference between the two techniques are presented and will be discussed later.

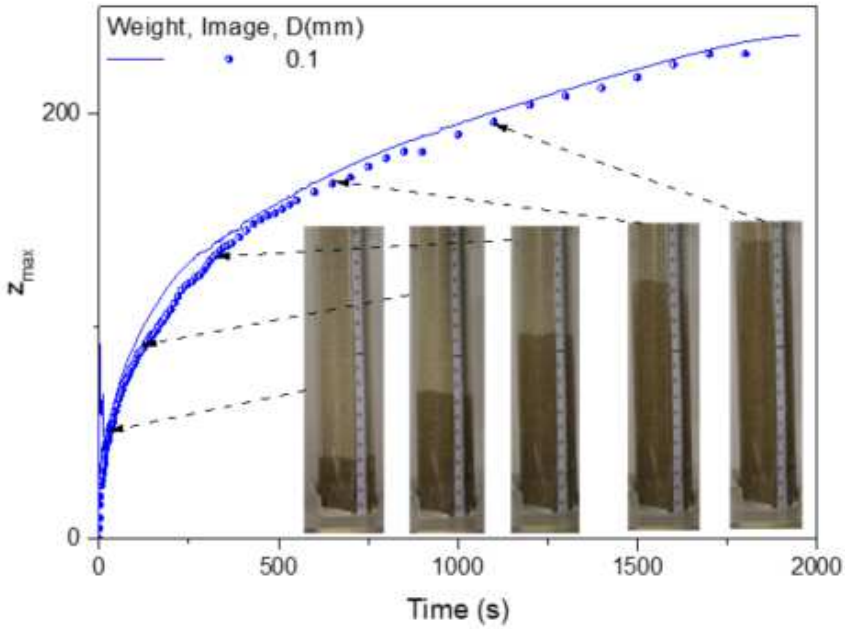

Figure 9. The liquid height rises for homogeneous domain, using the image processing (the discrete dots), and weighting techniques (the continuous line). The inserted chosen images are at the time points of 70s (5cm), 140s (9.5cm), 280s (13cm), 560s (16.5cm) and 1120s(19cm), respectively

Figure 10 summarizes the obtained results of height evolution for homogeneous sands of different sizes within the analysed domain. This figure represents also both the visually capillary rise height and the height deduced from the obtained weight evolutions. As expected, the increasing water content and the capillary rise heights for each sand dimension are in inverse proportion to the capillary dimension, which means the smaller the capillary diameter, the higher is the equilibrium height of the liquid rise.

It is important to mention that during the transient period, the water absorption rate for bigger sands is faster than the smaller ones. The rise speed decays later and the smaller size retrieves its higher rise ability. Therefore, the smaller size allows higher final rise and bigger diameter exhibits faster rise in the early time. Such difference of speed rise was introduced previously and it is a consequence of geometrical aspect.

Concerning shear stress during capillary rise, under the condition of the same bulk volume, the specific surface area of fine sands is much bigger than that of the coarse sands, which contributes to the increase of the shear stress. We have the theoretical support that macro pores are responsible for diffusion during the short time and micro pores are responsible for diffusion during the long time [19]. The optical technique and mass recording results agree well on the evolution behaviour, while the minor difference could be consequences of:

- the downside perturbation which is a consequence of the initial contact of the porous media and the horizontal liquid free surface (feeding tank)

- the non-flat liquid rising on the upper surface. We attribute partially this difference to the change in porosity at the wall-sand vicinity of the box.

The second point is confirmed by the difference of the continuous evolving between the final steady state of liquid height obtained by the sensor technique and the optical one (external surface), which is the consequence of this extra capillaries rising liquid.

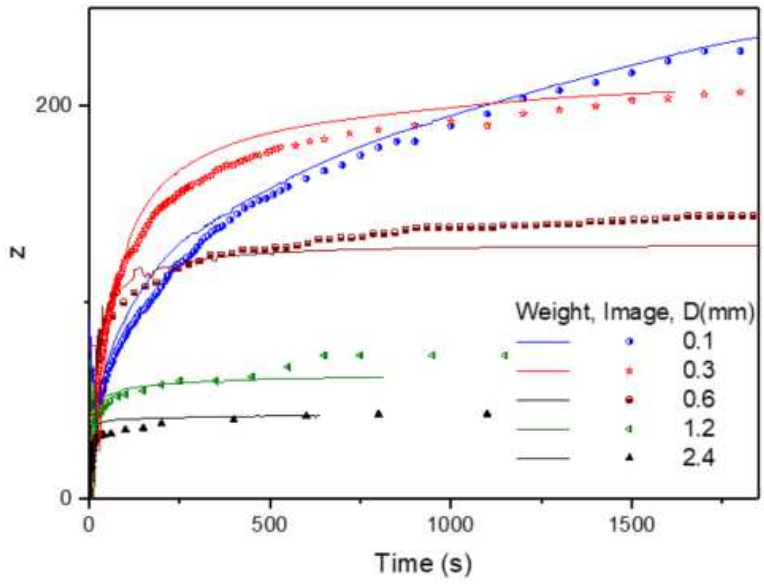

Figure 10. The height liquid rises versus time for different homogeneous domain, using both the image processing (dots) and weighting technique (lines)

The final reached steady height for the different equivalent capillary radius is represented in Fig. 11. The analytical estimation height is also compared in the same figure. The final height shows a good agreement and confirms the validity of using such modified equivalent radius to estimate the maximum liquid rise in steady state. Some errors remain as previously discussed and we underline that for the very fine sand the time to reach the experimentally steady state becomes so long that we use an extrapolating filling curves to extract the corresponding value. We presented the obtained imbibition results for the homogeneous domain. It allows the validation of our experimental, as well as the equivalent capillary diameter deduced from the sands.

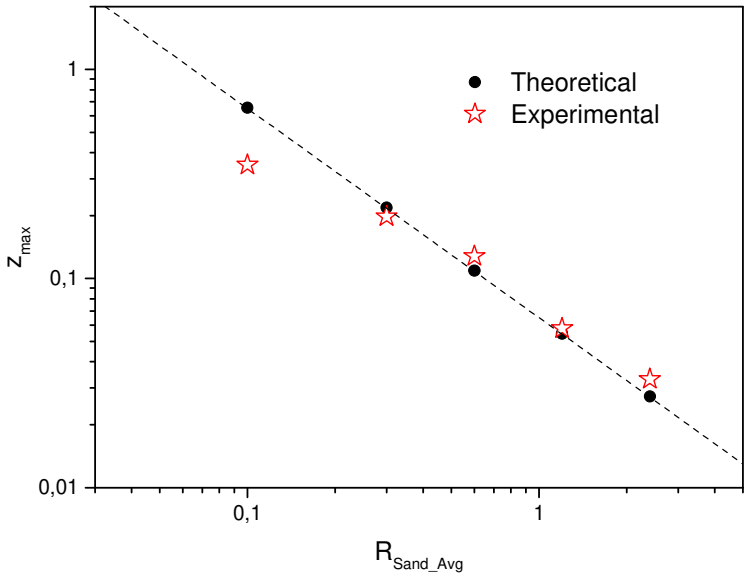

Figure 11. The effect of sand equivalent radius on the maximum liquid height rise (homogeneous domain)

The obtained experimental height rise appears to vary linearly to $\sqrt{t}$ and it is coherent with the analytical solution in the intermediate time and the considered experimental values of Ω . The vertical velocity is deduced to the variation as $V_v \sim 1/\sqrt{t}$. For heterogeneous domain, and as presented in Eq. (8), the horizontal pressure difference induces velocity excess, which is given by:

$$(V_v)_+ = \left(\frac{d\tilde{z}_1}{d\tilde{t}}\right)_+ = -(Bo_1)^{-5/2}\sqrt{Ga_1}\ Bn_1.\left(\frac{1}{\tilde{z}_1} - \frac{R_{rel}}{cos\theta_{rel}}\frac{1}{\tilde{z}_2}\right)\tilde{z}_{min}^2$$

Comparing this excess of vertical velocity to normal rise velocity, $V_v/(V_v)_+$ is the dimensionless number expressing the coupling phenomena level. This coupling is controlled by the two parameters ($\Omega; Bo$) and the ratio of the two adjacent layer geometrical characteristics, low coupling of the two-layer resistance (permeability) Bn_1 and the surface connecting $\tilde{e}$.

As previously underlined the speed to reach the final maximum z_{mx} is higher for bigger size of sand especially during the early time. We will analyse the coupling between the different adjacent layers in order to check the filling enhancement in the vertical multilayer case. We will analyse and discuss firstly the evolutions in a double layer test then a six – layer experiment.

Similar to the previous analysis for monolayer (homogeneous), we will present in this part the obtained results for the multilayer case (heterogeneous). As previously considered, the initial time is the very first moment that the liquid in the container gets in contact with the lower part of the sand domain. Fig. 12 presents the obtained results for the heterogeneous bilayer (0.3 mm and 0.6 mm) and the correspondingly separated homogeneous case. We retrieve the previous tendency obtained in the homogeneous case and in the previous model.

As showed in Fig. 12, during the transient period, the water imbibition rate for 0.6 mm is faster than for 0.3 mm. The rise speed decays later and the smaller size retrieves its ability of higher capillary rise. The heterogeneous case is represented by bigger half solid dots (see Fig. 12a). The 0.6 mm sands evolve almost identically to the homogeneous case (discussed in section analytically) and the 0.3 mm sands exhibit a faster liquid rise due to the coupling. A series of images during the test are selected to illustrate the coupled evolution and the feeding of water from 0.6 mm (the left side in bilayer images) 0.3 mm (the right side in bilayer images). The coupling is also illustrated by the irregular shape of the upper liquid surface.

We have access to the external surface observation but the liquid level is not necessarily the same on a horizontal interface plan. We can validate the obtained observation results by using the weighting (liquid mass evolution) techniques and the conversion of the equivalent obtained volume (z_1 and z_2) into mass. We plot such obtained equivalent mass by using the base surface of the media and its porosity. The results are plotted in Fig. 12b. This first heterogeneous bilayer domain (0.3 mm and 0.6 mm) exhibits a validation of the two used techniques (weight evolution of the absorbed liquid and the deduced mass from the two obtained height of the two layers, Fig. 11a).

The evolution of rising fluid over time is confirmed, as well as the final height position or mass in the steady state. We observe that the optical technique induces artefact, which could be a consequence of thin layer wetting rising along the external surfaces of the domain, and it is similar to what we got in the first homogeneous case.

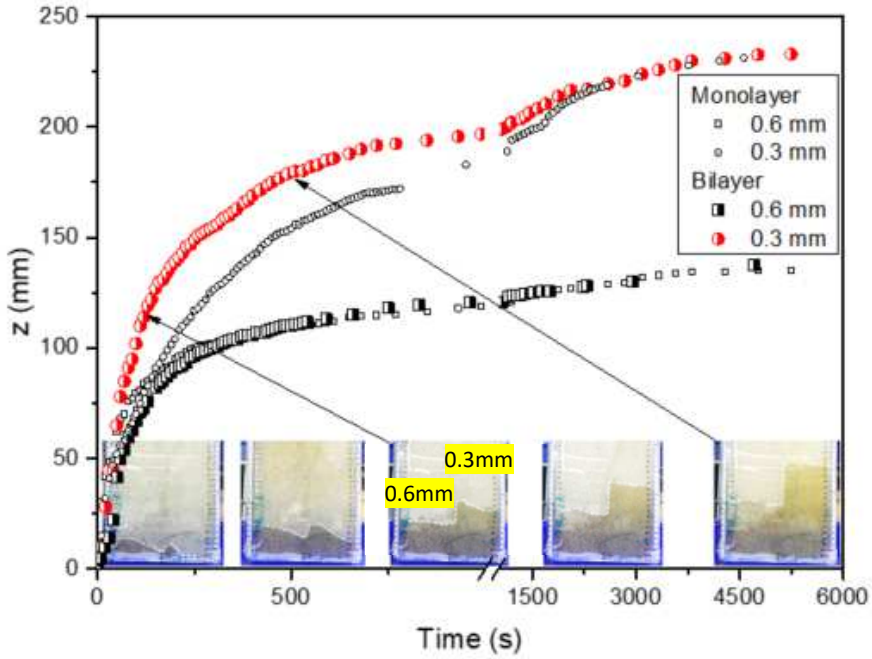

a)

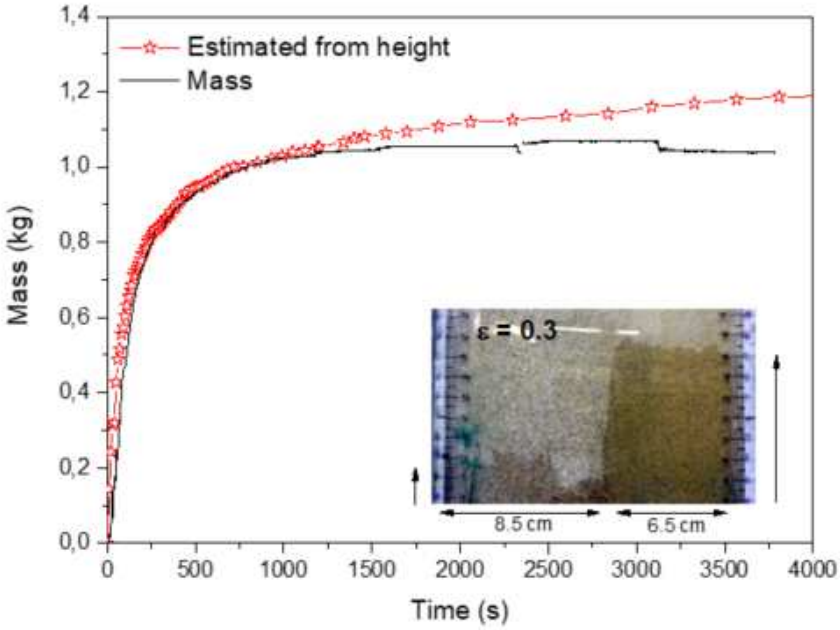

b)

Figure 12. The liquid height rises for the heterogeneous bilayer domain a), and the corresponding mass evolution, image processing in dots and the lines are for weighting technique b)

These interesting results of enhancing speed liquid rise in small equivalent capillaries will not overcome the maximum second fast rising layer (bigger diameter) and limited by the horizontal feeding velocity consequence of flow resistance (permeability and layer thickness). This flow resistance increases with the layer thickness and we will analyse this effect (thickness: 2.5 cm to 7 cm) in the following discussions.

To explore and generalize this observation we continue analysing a heterogeneous domain of multiple layers (six) as illustrated in Fig. 13. It is described in Fig. 13a the successive filling layout to get the six parallel layers with each layer thickness of 2.5 cm, and covering the diameters of 0.1 mm, 0.3 mm, 0.6 mm, 1.2 mm, 2.4 mm and 4.8mm. The photo of sands layout before and after the imbibition test are presented in Fig. 13b and Fig. 13c, respectively.

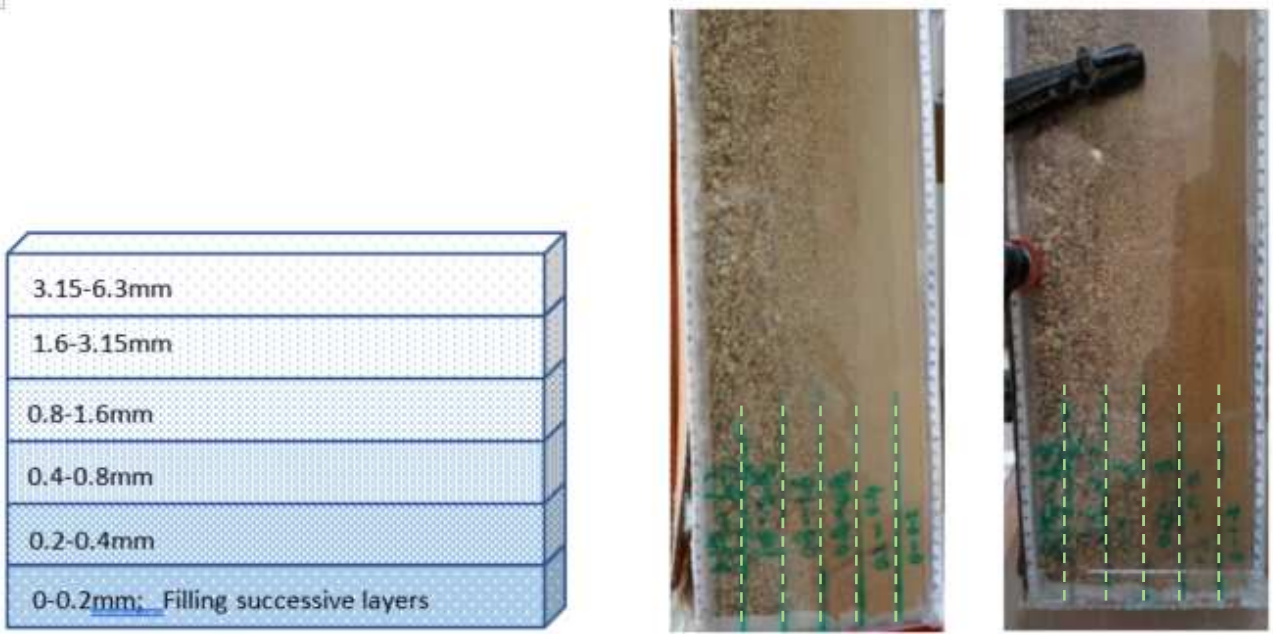

Figure. 13: Heterogeneous domain of six layers with sand diameters of 0.1 mm, 0.3 mm, 0.6 mm, 1.2 mm, 2.4 mm and 4.8 mm a), the vertical domain before imbibition b) and after imbibition c)

Figure 14 presents the results for the heterogeneous multilayer (from 0.1 mm to 4.8 mm) and the reference homogeneous case corresponding to 0.1 mm. We retrieve the previous tendency obtained in the bilayer case and in the previous model (coupled equivalent capillaries). The same results are observed as in the bilayer tests that during the transient period, the water absorption rate for bigger diameter is faster than smaller diameters and the bigger diameter is able to exchange and feed the adjacent layer of smaller diameters. The rise speed decays later and the smaller size retrieves successively its higher rise ability. A series of images are included in Fig. 14 to present the reached height level of liquid rise on the successive layers. It is indicated that the consecutive layers are of same liquid height for given time and when a layer becomes closer to its own maximum height it stops evolving and the other adjacent (right) layer follows the trend. This phenomenon is observed from bigger diameter to smaller one (from left to right).

The homogeneous case is represented by bigger black stars and dashed line in Fig. 14. The 0.1 mm exhibits a faster liquid rise and almost identical to the 0.3 mm on large time duration. The 0.3 mm was followed by the 0.6 mm tendency which lasts for a shorter time. Fig. 14 confirms again the strong enhancement in liquid speed filling as the 0.1 mm in heterogeneous case (red stars dots) reach the 200 mm height in 250 s instead of the 1200 s for the homogeneous case (black stars dots for homogenous case of 0.1 mm).

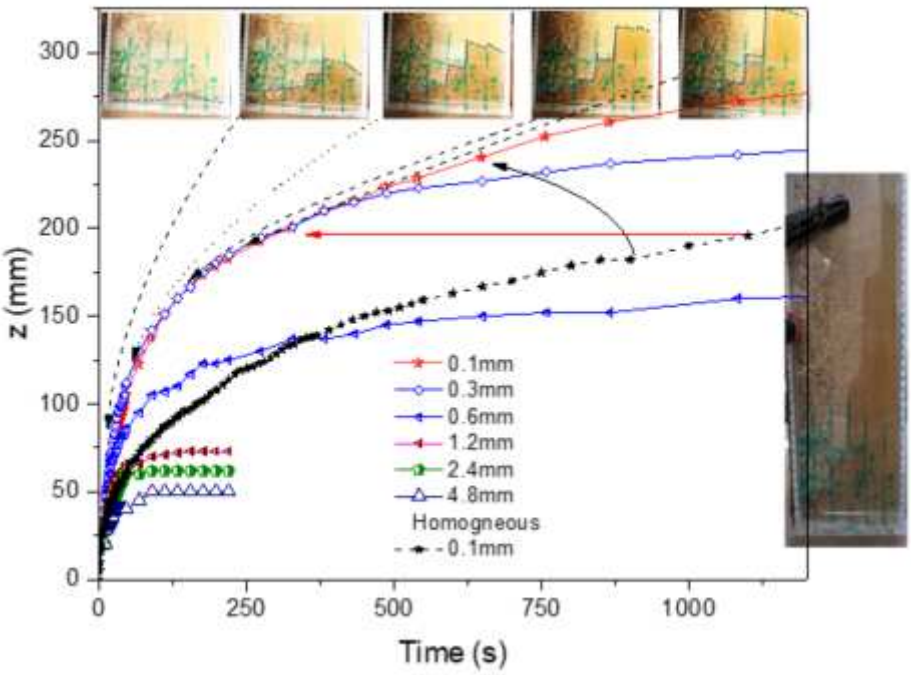

Figure 14. Liquid height rises for heterogeneous multilayer domain and the corresponding reference of homogeneous 0.1 mm case, images inserts illustrate the top shape of the liquid rise over such heterogenous domain.

From the results of heterogeneous case, it can be indicated that for two adjacent layers, there is the maximum height difference that can be reached, and the angle between the two heights is almost a right angle, as shown in the insert graphs of Fig. 14. The reader can mention such a surprising behaviour as we will get horizontal pressure gradient. It can be explained firstly that the capillary rise has reached its maximum height (for example z_{max1} and z_{max2}) because of the surface tension and corresponding equivalent radius. The layer which is finer in particle size absorbs water from the adjacent layer which has larger particle size, and the system will ultimately reach an equilibrium. Towards the tendency of minimizing the pressure difference and the gravity, an overall curvature is drawn and ensures the transition between the part of the fluid of the two successive layers.

On the other hand, in the second analysis we can argue that the capillaries could adjust the curvature on local capillaries diameter to equilibrate the gravity effect at given height without exchanging with the adjacent layer. We mentioned several times during the comparison of our two techniques for mass (or height) evolution that the liquid is wetting the box border and by capillary effect it allows the liquid to continue moving along the border and changing the appearance (optical technique) without varying the mass evolution (added liquid). Such artefact is also observed in this last test, especially in the longer time where the initially parallel clear liquid column rises on each layer with almost perpendicular transition progressively become a transition zone with curvature, as presented in Fig. 15.

The rise improvement for heterogenous cases (corresponding to equivalent capillary rise and capillary rise with layer exchanges) has been demonstrated explicitly and quantified experimentally and analytically. The interaction between these layers demonstrates how the cooperation appears in nature in order to fit with the optimal situation of fast filling the porous media or the equivalent in drying. Experimental results have favourable accordance with the theoretical analysis and the enhancement in imbibition has been demonstrated and explained as well.

The imbibition, as previously mentioned, is more complex when evaporation occurs in nature due to the salt deposition in more complex heterogeneous structure[38]. In some other application such deposition is used to repair the disorder in porous material such as in buildings[39].

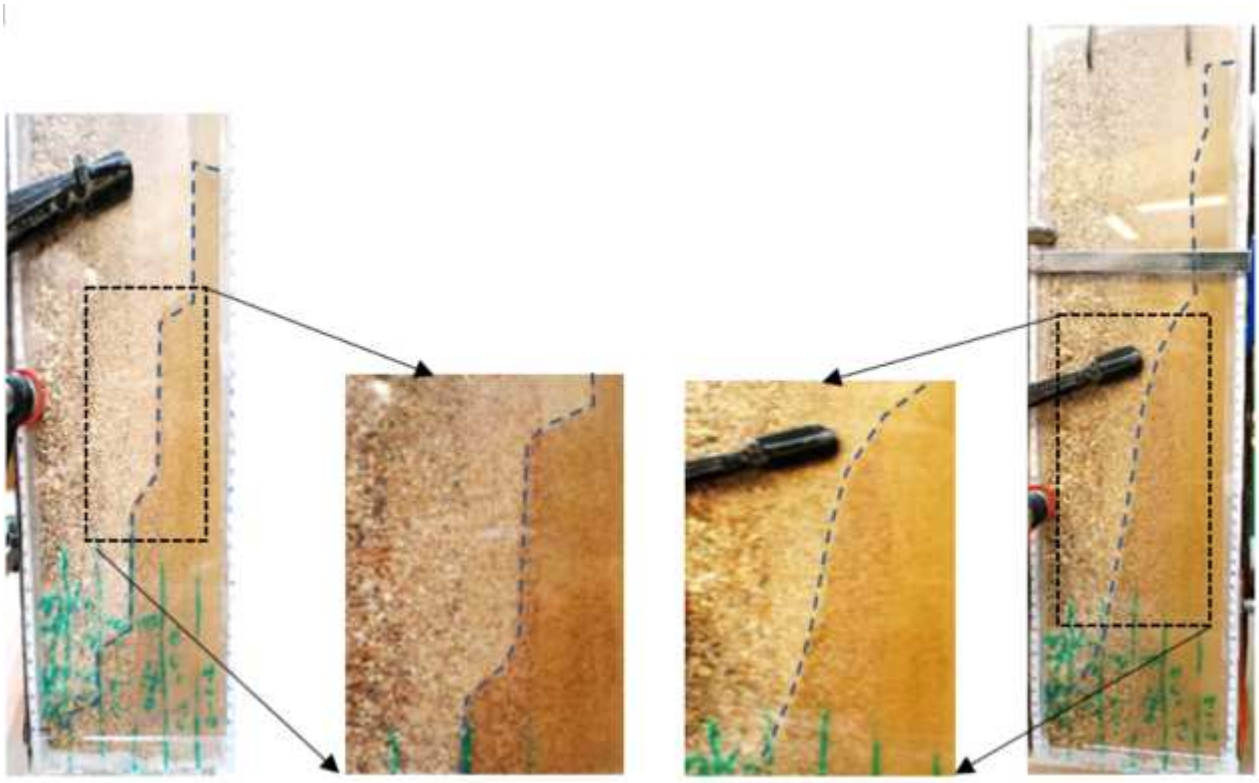

Figure 15. Liquid rise interface shape at two different time points (early – left and later – right), and their corresponding zooms (in central position)

CONCLUSION

This work allows to have a better understanding of flow mechanism in porous media for imbibition or drying process. A combination of experimental methods with single or multilayers is performed to investigate the dynamic capillary rise in such porous media. The procedure provides effective approaches to analyse both homogeneous and heterogeneous domains in permeability. The first part has led us to synthesize bibliographic information on geometric properties and capillary rises in porous media. The second part concerns the study of the capillary rise for the homogeneous and heterogeneous domains for different granulometry and surface tension. In summary, the smaller size or the higher surface tension will lead to a higher height of the capillary lift. On the other hand, the evolution of absorbed water illustrates more complex trends over time. The control and the prediction of the liquid content will allow to quantify the intra-capillary forces and thus to get access to the internal forces governing the water displacement in materials.

The practical significance of this work also lies in clarifying the establishment of a controlled protocol, the design and realization of the test benchmark. This will allow the continuity of the action and the understanding of the competition of the capillary rises in more complex heterogeneous domains coupled with a surface evaporation. These phenomena of liquid penetration will also explain the origin of disorders for structures above ground (building, support structures, *etc.*) as well as underground structures (tunnels, deep foundations, *etc.*), and also serve as a criterial of judging when liquid rise is feeding evaporating interfaces.

Nomenclature

Bo	Bond number	-
Bn_1	Flow coupling through the two-layer resistance (permeability)	
$\tilde{e}$	Dimension	
g	Gravity acceleration	$m \cdot s^{-2}$
Ga	Galileo number	
M_T	Mass in tube	kg
M_C	Mass in cap close to the tube	kg
M_∞	Mass in connecting area, tube vicinity to infinity	kg
P	Pressure	Pa
Qv	Volume flux	
R	Radius	m
R_{cap}	Equivalent capillary radius	
R_i, R_e	Double radii curvature of the liquid interface	m
$\mathcal{R}_{eq}$	Equivalent hydraulic resistance	
S	Surface	m^2
t	Time	s
$\tilde{t}$	Dimensionless time	-
t_r	Reference time	s
t_{r1}	Inertial reference time	s
t_{r2}	Shear reference time	s
t_{dif}	Diffusive reference time	s
V_{int}	Interface velocity (horizontal permeability)	$m \cdot s^{-1}$
z	Vertical capillary height	m
z_{mx}	Maximum capillary height in steady state	m

$\tilde{z}$	Dimensionless capillary height	-
$\dot{\tilde{z}}$	Dimensionless capillary rise speed	-
$\ddot{\tilde{z}}$	Dimensionless capillary rise acceleration	-
ε	Porosity	
$\Delta P_{c1/2\_int}$,	Pressure difference between capillary center and interface	Pa
θ	Contact angle	
μ	Dynamic viscosity	$Pa \cdot s$
ν	Kinematic viscosity	$m^2 \cdot s^{-1}$
Ω	Dimensionless number	
ρ	Liquid density	$kg \cdot m^{-3}$
σ	The surface tension of the liquid	$N \cdot m^{-1}$N
τ_{cis}	Shear stress	$N \cdot m^{-2}$

References

[1] M. Rosello, S. Sur, B. Barbet, and J. P. Rothstein, “Dripping-onto-substrate capillary breakup extensional rheometry of low-viscosity printing inks,” *J. Nonnewton. Fluid Mech.*, vol. 266, no. June, pp. 160–170, 2019, doi: 10.1016/j.jnnfm.2019.03.006.

[2] Y. Wang, R. Deng, L. Yang, and C. D. Bain, “Fabrication of monolayers of uniform polymeric particles by inkjet printing of monodisperse emulsions produced by microfluidics,” *Lab Chip*, vol. 19, no. 18, pp. 3077–3085, 2019, doi: 10.1039/C9LC00588A.

[3] B. Dai *et al.*, “Bioinspired Janus Textile with Conical Micropores for Human Body Moisture and Thermal Management,” *Adv. Mater.*, vol. 31, no. 41, p. e1904113, 2019, doi: 10.1002/adma.201904113.

[4] B. Xiao, J. Fan, and F. Ding, “Prediction of Relative Permeability of Unsaturated Porous Media Based on Fractal Theory and Monte Carlo Simulation,” *Energy & Fuels*, vol. 26, no. 11, pp. 6971–6978, Nov. 2012, doi: 10.1021/ef3013322.

[5] Y.-J. Lin *et al.*, “Characterizing Asphaltene Deposition in the Presence of Chemical Dispersants in Porous Media Micromodels,” *Energy & Fuels*, vol. 31, no. 11, pp. 11660–11668, Nov. 2017, doi: 10.1021/acs.energyfuels.7b01827.

[6] S. Saraji, L. Goual, and M. Piri, “Adsorption of Asphaltenes in Porous Media under Flow Conditions,” *Energy & Fuels*, vol. 24, no. 11, pp. 6009–6017, Nov. 2010, doi: 10.1021/ef100881k.

[7] M. Singh, N. V. Datla, S. Kondaraju, and S. S. Bahga, “Enhanced thermal performance of micro heat pipes through optimization of wettability gradient,” *Appl. Therm. Eng.*, vol. 143, pp. 350–357, 2018, doi: https://doi.org/10.1016/j.applthermaleng.2018.07.093.

[8] M. A. Chernysheva and Y. F. Maydanik, “Simulation of heat and mass transfer in a cylindrical evaporator of a loop heat pipe,” *Int. J. Heat Mass Transf.*, vol. 131, pp. 442–449, 2019, doi: https://doi.org/10.1016/j.ijheatmasstransfer.2018.11.034.

[9] B. XIAO *et al.*, “A NOVEL FRACTAL MODEL FOR RELATIVE PERMEABILITY OF GAS DIFFUSION LAYER IN PROTON EXCHANGE MEMBRANE FUEL CELL WITH CAPILLARY PRESSURE EFFECT,” *Fractals*, vol. 27, no. 02, p. 1950012, Sep. 2018, doi: 10.1142/S0218348X19500129.

[10] P. Carrere and M. Prat, “Liquid water in cathode gas diffusion layers of PEM fuel cells: Identification of various pore filling regimes from pore network simulations,” *Int. J. Heat Mass Transf.*, vol. 129, pp. 1043–1056, 2019, doi: https://doi.org/10.1016/j.ijheatmasstransfer.2018.10.004.

[11] Y. Liu, J. Kaszuba, and J. Oakey, “Microfluidic investigations of crude oil-brine interface elasticity modifications via brine chemistry to enhance oil recovery,” *Fuel*, vol. 239, pp. 338–346, 2019, doi: https://doi.org/10.1016/j.fuel.2018.11.040.

[12] R. Gharibshahi, M. Omidkhah, A. Jafari, and Z. Fakhroueian, “Hybridization of superparamagnetic Fe3O4 nanoparticles with MWCNTs and effect of surface modification on electromagnetic heating process efficiency: A microfluidics enhanced oil recovery study,” *Fuel*, vol. 282, p. 118603, 2020, doi: https://doi.org/10.1016/j.fuel.2020.118603.

[13] C. Carrell *et al.*, “Beyond the lateral flow assay: A review of paper-based microfluidics,” *Microelectron. Eng.*, vol. 206, pp. 45–54, 2019, doi: https://doi.org/10.1016/j.mee.2018.12.002.

[14] F. Schaumburg and C. L. A. Berli, “Assessing the rapid flow in multilayer paper-based microfluidic

devices," *Microfluid. Nanofluidics*, vol. 23, no. 8, p. 98, 2019, doi: 10.1007/s10404-019-2265-3.

[15] J.-H. Lin, W.-H. Chen, Y.-J. Su, and T.-H. Ko, "Performance Analysis of a Proton-Exchange Membrane Fuel Cell (PEMFC) with Various Hydrophobic Agents in a Gas Diffusion Layer," *Energy & Fuels*, vol. 22, no. 2, pp. 1200–1203, Mar. 2008, doi: 10.1021/ef7007024.

[16] K. K. Lee, M.-O. Kim, and S. Choi, "A whole blood sample-to-answer polymer lab-on-a-chip with superhydrophilic surface toward point-of-care technology," *J. Pharm. Biomed. Anal.*, vol. 162, pp. 28–33, 2019, doi: 10.1016/j.jpba.2018.09.007.

[17] H.-A. Joung *et al.*, "Paper-based multiplexed vertical flow assay for point-of-care testing," *Lab Chip*, vol. 19, no. 6, pp. 1027–1034, 2019, doi: 10.1039/C9LC00011A.

[18] R. Lucas, "Ueber das Zeitgesetz des kapillaren Aufstiegs von Flüssigkeiten," *Kolloid-Zeitschrift*, vol. 23, no. 1, pp. 15–22, Jul. 1918, doi: 10.1007/BF01461107.

[19] E. W. Washburn, "The Dynamics of Capillary Flow," *Phys. Rev.*, vol. 17, no. 3, pp. 273–283, Mar. 1921, doi: 10.1103/PhysRev.17.273.

[20] J. M. Bell and F. K. Cameron, "The flow of liquids through capillary spaces," *J. Phys. Chem.*, vol. 10, no. 8, pp. 658–674, 1905, doi: 10.1021/j150080a005.

[21] M. D. and R. S. S. James Jurin, "II. An account of some experiments shown before the Royal Society; with an enquiry into the cause of the ascent and suspension of water in capillary tubes," *Philos. Trans. R. Soc.*, vol. 30, no. 355, pp. 739–747, 1719.

[22] J. Szekely, A. W. Neumann, and Y. K. Chuang, "The rate of capillary penetration and the applicability of the washburn equation," *J. Colloid Interface Sci.*, vol. 35, no. 2, pp. 273–278, Feb. 1971, doi: 10.1016/0021-9797(71)90120-2.

[23] M. Stange, M. E. Dreyer, and H. J. Rath, "Capillary driven flow in circular cylindrical tubes," *Phys. Fluids*, vol. 15, no. 9, pp. 2587–2601, Sep. 2003, doi: 10.1063/1.1596913.

[24] D. Quéré, "Inertial capillarity," *Europhys. Lett.*, vol. 39, no. 5, pp. 533–538, Sep. 1997, doi: 10.1209/epl/i1997-00389-2.

[25] N. Fries and M. Dreyer, "Dimensionless scaling methods for capillary rise," *J. Colloid Interface Sci.*, vol. 338, no. 2, pp. 514–518, Oct. 2009, doi: 10.1016/j.jcis.2009.06.036.

[26] B. H. Sun, "Singularity-free approximate analytical solution of capillary rise dynamics," *Sci. China Physics, Mech. Astron.*, vol. 61, no. 8, 2018, doi: 10.1007/s11433-018-9247-1.

[27] S. Pavuluri, J. Maes, and F. Doster, "Spontaneous imbibition in a microchannel: analytical solution and assessment of volume of fluid formulations," *Microfluid. Nanofluidics*, vol. 22, p. 90, 2018, doi: 10.1007/s10404-018-2106-9.

[28] D. Gründing *et al.*, "A comparative study of transient capillary rise using direct numerical simulations," *Appl. Math. Model.*, vol. 86, pp. 142–165, Oct. 2020, doi: 10.1016/j.apm.2020.04.020.

[29] S. hua YIN, L. ming WANG, X. CHEN, and A. xiang WU, "Effect of ore size and heap porosity on capillary process inside leaching heap," *Trans. Nonferrous Met. Soc. China (English Ed.*, vol. 26, no. 3, pp. 835–841, Mar. 2016, doi: 10.1016/S1003-6326(16)64174-2.

[30] F. Xiao and X. Yin, "Geometry models of porous media based on Voronoi tessellations and their porosity-permeability relations," in *Computers and Mathematics with Applications*, Jul. 2016, vol. 72, no. 2, pp. 328–348, doi: 10.1016/j.camwa.2015.09.009.

[31] C. H. Arns, M. A. Knackstedt, W. V. Pinczewski, and N. S. Martys, “Virtual permeametry on microtomographic images,” *J. Pet. Sci. Eng.*, vol. 45, no. 1–2, pp. 41–46, 2004, doi: 10.1016/j.petrol.2004.05.001.

[32] C. K. CHEN and S. W. HSIAO, “TRANSPORT PHENOMENA IN ENCLOSED POROUS CAVITIES,” D. B. INGHAM and I. B. T.-T. P. in P. M. POP, Eds. Oxford: Pergamon, 1998, pp. 31–56.

[33] E. K. Rideal, “CVIII. *On the flow of liquids under capillary pressure*,” *London, Edinburgh, Dublin Philos. Mag. J. Sci.*, vol. 44, no. 264, pp. 1152–1159, Dec. 1922, doi: 10.1080/14786441008634082.

[34] K. Liang *et al.*, “Study on two-dimensional capillary water rise in cracked and uncracked cement based materials,” *Constr. Build. Mater.*, vol. 265, p. 120310, 2020, doi: https://doi.org/10.1016/j.conbuildmat.2020.120310.

[35] M. Stange, M. E. Dreyer, and H. J. Rath, “Capillary driven flow in circular cylindrical tubes,” *Phys. Fluids*, vol. 15, no. 9, pp. 2587–2601, 2003, doi: 10.1063/1.1596913.

[36] Dani Or; Markus Tuller; Jon M. Wraith, “Soil Water Potential.” pp. 1–13, 2003.

[37] R. P. Dias, J. A. Teixeira, M. G. Mota, and A. I. Yelshin, “Particulate Binary Mixtures: Dependence of Packing Porosity on Particle Size Ratio,” *Ind. Eng. Chem. Res.*, vol. 43, no. 24, pp. 7912–7919, Nov. 2004, doi: 10.1021/ie040048b.

[38] E. Franzoni and S. Bandini, “Spontaneous electrical effects in masonry affected by capillary water rise: The role of salts,” *Constr. Build. Mater.*, vol. 35, pp. 642–646, 2012, doi: https://doi.org/10.1016/j.conbuildmat.2012.04.098.

[39] O. Rozenbaum, S. Anne, and J.-L. Rouet, “Modification and modeling of water ingress in limestone after application of a biocalcification treatment,” *Constr. Build. Mater.*, vol. 70, pp. 97–103, 2014, doi: https://doi.org/10.1016/j.conbuildmat.2014.07.038.